RSC Advances

PAPER

View Article Online
View Journal | View Issue

Cite this: *RSC Adv.*, 2015, **5**, 58694

The beneficial effects of trifluoromethyl-substituents on the photoconversion efficiency of copper(I) dyes in dye-sensitized solar cells†

Fabian Brunner, Y. Maximilian Klein, Sarah Keller, Collin D. Morris, Alessandro Prescimone, Edwin C. Constable and Catherine E. Housecroft*

The synthesis and characterization of $[Cu(\mathbf{2})_2][PF_6]$ and $[Cu(\mathbf{3})_2][PF_6]$ in which **2** = 6,6′-bis(trifluoromethyl)-2,2′-bipyridine and **3** = 6-trifluoromethyl-2,2′-bipyridine are reported. The single crystal structure of $[Cu(\mathbf{2})_2][PF_6]$ confirms that the copper(I) centre is sterically protected by the four CF_3 groups in a near regular tetrahedral environment. The Cu^+/Cu^{2+} oxidation potential is shifted from +0.44 to +0.72 V on going from $[Cu(\mathbf{1})_2][PF_6]$ to $[Cu(\mathbf{2})_2][PF_6]$ (**1** = 6,6′-dimethyl-2,2′-bipyridine), in keeping with the electron-withdrawing effects of the CF_3 groups. ^1H and ^{19}F NMR spectroscopic data for a CH_2Cl_2 solution containing $[Cu(\mathbf{1})_2][PF_6]$ and $[Cu(\mathbf{2})_2][PF_6]$ demonstrate that the ligands in $[Cu(\mathbf{2})_2][PF_6]$ remain highly labile. An on-surface procedure was used to assemble the dyes $[Cu(\mathbf{4})(\mathbf{2})]^+$ and $[Cu(\mathbf{4})(\mathbf{3})]^+$ (**4** = anchoring ligand ((6,6′-dimethyl-[2,2′-bipyridine]-4,4′-diyl)bis(4,1-phenylene))bis(phosphonic acid)) on TiO_2; solid-state absorption spectra show that dye coverage for $[Cu(\mathbf{4})(\mathbf{3})][PF_6]$ exceeds that of $[Cu(\mathbf{4})(\mathbf{2})][PF_6]$. The performances of the dyes in dye-sensitized solar cells (DSCs) are compared with that of $[Cu(\mathbf{4})(\mathbf{1})]^+$. DSCs containing the fluorinated ancillary ligands exhibit photoconversion efficiencies of ≈30–34% relative to N719 set at 100%; this is a significant enhancement with respect to DSCs containing $[Cu(\mathbf{4})(\mathbf{1})]^+$ with no fluoro-groups. Density functional theory (DFT) calculations for the heteroleptic dyes demonstrate that the HOMO is stabilized upon introduction of the CF_3 groups, but that the compositions of the molecular orbitals in the HOMO–LUMO manifold are little changed. The improved DSC performance is associated with enhanced short-circuit current density (J_{SC}) for $[Cu(\mathbf{4})(\mathbf{3})]^+$ and $[Cu(\mathbf{4})(\mathbf{2})]^+$ *versus* $[Cu(\mathbf{4})(\mathbf{1})]^+$; this is also seen in high EQE_{max} values of 46% for $[Cu(\mathbf{4})(\mathbf{2})]^+$ and 51% for $[Cu(\mathbf{4})(\mathbf{3})]^+$ (both at λ_{max} = 480 nm).

Received 21st May 2015
Accepted 30th June 2015

DOI: 10.1039/c5ra09590e

www.rsc.org/advances

Introduction

The replacement of rare elements by Earth-abundant metals in dye-sensitized solar cells (DSCs),[1,2] organic light-emitting diodes (OLEDs),[3,4] and light-emitting electrochemical cells (LECs)[5] is a high priority for developing sustainable materials chemistry. Although ruthenium, metal porphyrin-based and metal-free organic compounds are state-of-the-art dyes with photoconversion efficiencies reaching ≈12%,[6] the last few years have seen significant progress in the use of copper(I) complexes in Grätzel-type[7] DSCs. Most attention has focused on the development of $[Cu(\hat{N}\hat{N})_2]^+$ complexes in which $\hat{N}\hat{N}$ is a 2,2′-bipyridine (bpy) or 1,10-phenanthroline (phen) domain. Early copper(I) dyes were homoleptic complexes bearing anchoring groups,[8–11] and such compounds continue to be used.[12] However, DSC performance benefits from the use of heteroleptic dyes $[Cu(L_{anchor})(L_{ancillary})]^+$. One ligand bears peripheral groups suited to binding to the semiconductor (TiO_2) surface, while functionalities in the second (ancillary) ligand can be freely varied (Scheme 1) allowing ready tuning of the photophysical properties of the dye.

Substituents adjacent to the *N*,*N*′-metal binding site in bpy and phen are essential for stabilizing tetrahedral copper(I) against oxidation to square planar copper(II).[13] However, unless these substituents are very sterically demanding, heteroleptic complexes rapidly establish an equilibrium mixture of homo- and heteroleptic complexes,[14] making synthesis and isolation of the latter challenging. Two independent strategies have emerged for the synthesis and surface-binding of heteroleptic copper(I) sensitizers. The first is the HETPHEN approach with bulky substituents adjacent to the *N*,*N*′-donor sites[15] allowing heteroleptic copper(I) dyes to be isolated and then adsorbed onto an electrode surface.[16,17] Using this approach, Boujtita, Odobel and co-workers have designed a dye with a landmark photon-to-current conversion efficiency of 4.66% (relative to 7.36% for ruthenium dye N719).[17] In the second approach, we

Department of Chemistry, University of Basel, Spitalstrasse 51, CH-4056 Basel, Switzerland. E-mail: catherine.housecroft@unibas.ch

† Electronic supplementary information (ESI) available: Fig. S1 ^{19}F NMR spectra of $[Cu(\mathbf{2})_2][PF_6]$ and $[Cu(\mathbf{3})_2][PF_6]$. CCDC 1062412. For ESI and crystallographic data in CIF or other electronic format see DOI: 10.1039/c5ra09590e

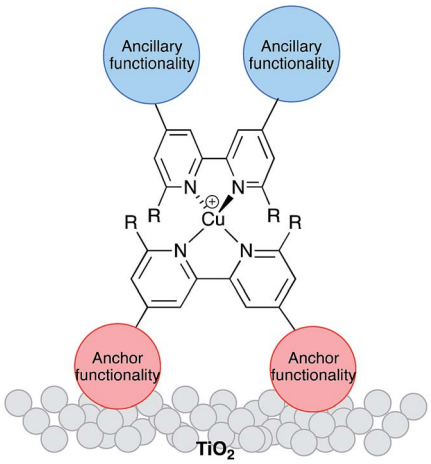

Scheme 1 Schematic representation of a surface-bound heteroleptic copper(I) sensitizer.

have introduced a stepwise, on-surface assembly in which the photoanode is first functionalized with an anchoring ligand, which then undergoes *in situ* ligand exchange with a homoleptic copper(I) complex (Scheme 2).[18,19] A variation of the latter is a one-pot approach, in which the ligand-functionalized electrode is soaked in a dye-bath comprising a 1 : 1 mixture of $[Cu(MeCN)_4][PF_6]$ and an ancillary ligand.[20] Both are straightforward and adaptable methods that allow fast throughput screening of combinations of L_{anchor} and $L_{ancillary}$ in $[Cu(L_{anchor})(L_{ancillary})]^+$ sensitizers. Using this approach, we have achieved photoconversion efficiencies of >3% (relative to 7.63% for reference dye N719).[21]

Given that surface-bound sensitizers are typically designed on a 'push–pull' principle,[22] it is somewhat surprising that the highest efficiencies (3.16%) for copper-based DSCs assembled by the on-surface approach are for dyes in which the ancillary ligands contain electron-withdrawing halo-substituents.[21] The results of ground state DFT calculations indicate that the incorporation of peripheral iodo-substituents in the dye may result in improved electron transfer from the reduced electrolyte over the halo-substituted aryl ring to the sensitizer.[21] More elaborately designed copper(I) dyes containing peripheral hole-transporting domains[20,23–25] failed to achieve efficiencies as high as those with halo-functionalities. Interestingly, the incorporation of fluorinated-substituents in both ruthenium(II) and organic dyes may impede charge recombination events.[26,27] We were therefore prompted to consider different ways in which halo-substituents could be incorporated into the ancillary ligand in a $[Cu(L_{anchor})(L_{ancillary})]^+$ sensitizer. One of the simplest ancillary ligands is 6,6′-dimethyl-2,2′-bipyridine (**1**, Scheme 3). The performances of cells incorporating $[Cu(L_{anchor})(\mathbf{1})]^+$ sensitizers are enhanced on going from L_{anchor} with carboxylic acid to phosphonic acid anchors, and by introducing an arene spacer between the bpy and phosphonic acid anchor domains.[28,29] Here, we report the effects of replacing **1** as the ancillary ligand by **2** or **3** which contain CF_3 groups in the 6- and 6′-positions of the bpy ligand (Scheme 3). The introduction of CF_3 substituents in the 2- and 9-positions in $[Cu(phen)_2]^+$ complexes has been investigated in detail,[30–33] and considerably stabilizes these complexes with respect to oxidation to copper(II).[30]

Experimental

General

A Bruker Avance III-400 or 500 NMR spectrometer was used to record ^1H, ^{13}C, ^{19}F and ^{31}P NMR spectra at 295 K. ^1H and ^{13}C chemical shifts were referenced to residual solvent peaks with respect to δ(TMS) = 0 ppm, ^{31}P with respect to δ(85% aqueous H_3PO_4) = 0 ppm, and ^{19}F with respect to an external reference of $CFCl_3$ (δ = 0 ppm). Solution and solid-state absorption spectra were recorded on an Agilent 8453 and Cary 5000 spectrophotometer, respectively; solid-state spectra were recorded in transmission mode. Electrospray ionization (ESI) and MALDI-TOF mass spectra were recorded on Bruker Esquire 3000plus and Bruker microflex FT instruments, respectively.

Electrochemical measurements were made using a CH Instruments 900B potentiostat with glassy carbon or platinum working electrode and platinum wire and silver wire as the

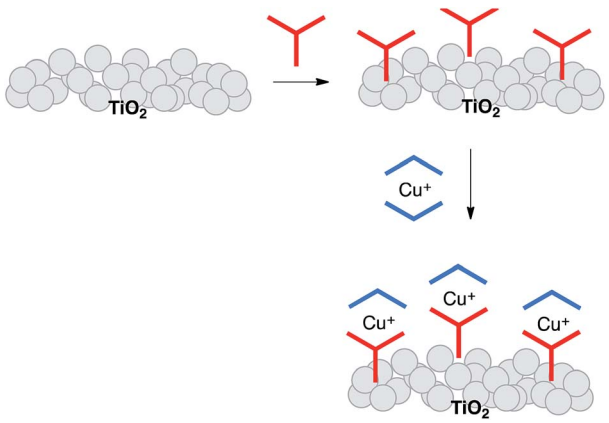

Scheme 2 Stepwise, on-surface assembly of a heteroleptic copper(I) dye.

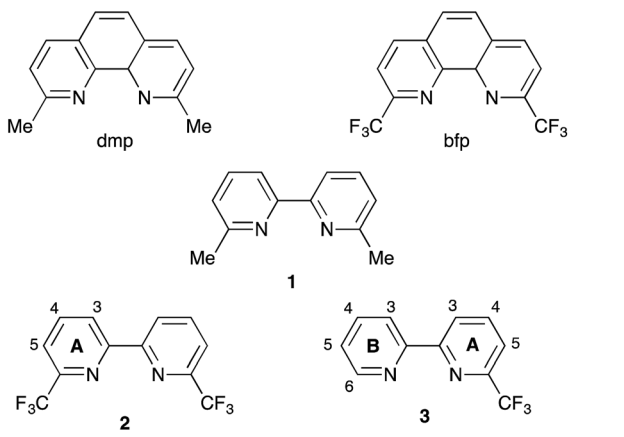

Scheme 3 Structures of ligands with numbering for NMR spectroscopic assignments in **2** and **3**.

counter and pseudo-reference electrodes, respectively. Substrates were dissolved in HPLC grade CH_2Cl_2 ($\approx 10^{-4}$ to 10^{-5} mol dm^{-3}) containing 0.1 mol dm^{-1} [^{n}Bu$_4$N][PF$_6$] as the supporting electrolyte; all solutions were degassed with argon. Cp_2Fe (Fc) was used as an internal or external reference (see text) and the scan rate was 100–300 mV s^{-1}.

A Biotage Initiator 8 was used for microwave reactions. Compound **2** was prepared according to the literature.[34] 2-Chloro-6-(trifluoromethyl)pyridine and 2-pyridylzinc bromide were purchased from Fluorochem and Merck, respectively. [Cu(MeCN)$_4$][PF$_6$] was prepared as previously reported.[35]

Compound 3. Solid 2-chloro-6-(trifluoromethyl)pyridine (423 mg, 2.33 mmol) and [Pd(PPh$_3$)$_4$] (135 mg, 0.12 mmol) were added to a 10–20 ml vial, and the tube was then evacuated and refilled with N_2 three times. Dry THF (5 ml) and a solution of 2-pyridylzinc bromide (0.5 M in THF, 7 ml, 3.50 mmol) were added, and then the tube was sealed, and heated in a microwave reactor at 110 °C for 2 h. The reaction mixture was poured into a separating funnel and saturated aqueous $NaHCO_3$ was added. The mixture was extracted with CH_2Cl_2 (3 × 50 ml), and then the combined organic layers were washed with water (2 × 100 ml) and dried over $MgSO_4$. The solvent was removed and the brown crude material was redissolved in CH_2Cl_2 and filtered over silica. The solvent was removed to give **3** as a white solid (318 mg, 1.42 mmol, 61%). ^{1}H NMR (400 MHz, $CDCl_3$) δ/ppm 8.69 (ddd, J = 4.7, 1.8, 0.9 Hz, 1H, H^{B6}), 8.64 (dt, J = 8.0, 0.8 Hz, 1H, H^{A3}), 8.53 (dt, J = 7.9, 1.1 Hz, 1H, H^{B3}), 7.99 (td, J = 7.8, 0.7 Hz, 1H, H^{A4}), 7.85 (td, J = 7.7, 1.8 Hz, 1H, H^{B4}), 7.69 (dd, J = 7.8, 1.0 Hz, 1H, H^{A5}), 7.36 (ddd, J = 7.5, 4.7, 1.2 Hz, 1H, H^{B5}). ^{13}C NMR (126 MHz, $CDCl_3$) δ/ppm 156.7 (C^{A2}), 154.8 (C^{B2}), 149.3 (C^{B6}), 148.0 (q, J_{CF} = 35 Hz, C^{A6}), 138.4 (C^{A4}), 137.3 (C^{B4}), 124.6 (C^{B5}), 123.6 (C^{A3}), 121.8 (C^{B3}), 121.7 (q, J = 274 Hz, C^{CF3}), 120.3 (q, J_{CF} = 2.9 Hz, C^{A5}). ^{19}F NMR (376 MHz, CD_2Cl_2) δ/ppm −68.4. ESI MS m/z 225.1 [M + H]$^+$ (base peak, calc. 225.2). UV-Vis (CH_2Cl_2, 2.5 × 10^{-5} mol dm^{-3}): λ/nm (ε/dm^3 mol^{-1} cm^{-1}) 238 (10 600), 245sh (9400), 282 (12 600), 295sh (6700). Found C 59.31, H 3.41, N 12.46; $C_{11}H_7F_3N_2$ requires C 58.93, H 3.15, N 12.50%.

[Cu(2)$_2$][PF$_6$]. [Cu(MeCN)$_4$][PF$_6$] (93 mg, 0.25 mmol) was dissolved in CH_2Cl_2 (25 ml) and **2** (146 mg, 0.50 mmol) was added. The mixture was stirred for 2 h at room temperature and then the orange solution was filtered and the solvent from the filtrate was removed under reduced pressure. The crude product was washed with Et_2O and cyclohexane to give [Cu(**2**)$_2$][PF$_6$] (86.0 mg, 0.108 mmol, 43.2%) as an orange crystalline solid. ^{1}H NMR (500 MHz, CD_2Cl_2) δ/ppm 8.70 (dd, J = 8.2, 1.0 Hz, 4H, H^{A3}), 8.44 (t, J = 8.0 Hz, 4H, H^{A4}), 8.07 (dd, J = 7.9, 1.0 Hz, 4H, H^{A5}). ^{13}C NMR (126 MHz, CD_2Cl_2) δ/ppm 152.8 (C^{A6}), 146.8 (C^{A2}) 141.3 (C^{A4}), 126.7 (C^{A3}), 125.0 (C^{A5}), 121.3 (q, J = 273 Hz, C^{CF3}). ^{19}F NMR (376 MHz, CD_2Cl_2) δ/ppm −68.2 (F^{CF3}), −73.3 (d, J_{PF} = 710 Hz, F^{PF6}). ^{31}P NMR (162 MHz, CD_2Cl_2) −144.0 (septet, J_{PF} = 710 Hz). MALDI-TOF MS m/z 647.2 [M − PF$_6$]$^+$ (base peak, calc. 647.0). UV-Vis (CH_2Cl_2, 2.5 × 10^{-5} mol dm^{-3}): λ/nm (ε/dm^3 mol^{-1} cm^{-1}) 273 (30 500), 295 (23 000), 340 (2980), 445 (7050). Found C 36.63, H 1.98, N 7.39; $C_{24}H_{12}CuF_{18}N_4P$ requires C 36.36, H 1.53, N 7.07%.

[Cu(3)$_2$][PF$_6$]. [Cu(MeCN)$_4$][PF$_6$] (93 mg, 0.25 mmol) and **3** (112.0 mg, 0.50 mmol) were dissolved in CH_2Cl_2 (25 ml) and the mixture was stirred for 1.5 h at room temperature. After filtration, the filtrate was collected and the solvent removed under reduced pressure. [Cu(**3**)$_2$][PF$_6$] was isolated as an orange crystalline solid (147 mg, 0.224 mmol, 89.6%).^{1}H NMR (500 MHz, CD_2Cl_2) δ/ppm 8.62 (m, 2H, H^{B6}), 8.58 (dd, J = 8.3, 1.0 Hz, 2H, H^{A3}), 8.43 (dt, J = 8.3, 1.0 Hz, 2H, H^{B3}), 8.33 (t, J = 8.0 Hz, 2H, H^{A4}), 8.19 (td, J = 7.9, 1.7 Hz, 2H, H^{B4}), 7.95 (dd, J = 7.8, 1.1 Hz, 2H, H^{A5}), 7.66 (ddd, J = 7.6, 5.1, 1.2 Hz, 2H, H^{B5}). ^{13}C NMR (126 MHz, CD_2Cl_2) δ/ppm 154.2 (C^{A6}), 151.0 (C^{B6}), 149.9 (C^{B2}), 146.4 (C^{A2}), 140.9 (C^{A4}), 139.2 (C^{B4}), 127.9 (C^{B5}), 125.5 (C^{A3}), 123.6 (C^{A5}), 123.4 (C^{B3}), 120.9 (q, J = 274 Hz, C^{CF3}). ^{19}F NMR (376 MHz, CD_2Cl_2) δ/ppm −68.5 (F^{CF3}), −73.3 (d, J_{PF} = 710 Hz, F^{PF6}). ^{31}P NMR (162 MHz, CD_2Cl_2) −144.0 (septet, J_{PF} = 710 Hz). MALDI-TOF MS m/z 511.1 [M − PF$_6$]$^+$ (base peak, calc. 511.0). UV-Vis (CH_2Cl_2, 2.5 × 10^{-5} mol dm^{-3}): λ/nm (ε/dm^3 mol^{-1} cm^{-1}) 263 (24 400), 273 (25 800), 293 (26 200), 340 (2940), 443 (6580). Found C 40.94, H 2.51, N 8.53; $C_{22}H_{14}CuF_{12}N_4P$ requires C 40.23, H 2.15, N 8.53%.

Crystallography. Single crystal data were collected on a Bruker APEX-II diffractometer; data reduction, solution and refinement used APEX.[36] Structure analysis used Mercury v. 3.5.1.[37]

[Cu(2)$_2$][PF$_6$]. $C_{24}H_{12}CuF_{18}N_4P$, M = 792.87, yellow-orange block, orthorhombic, space group $P2_12_12_1$, a = 12.9418(10), b = 13.3852(11), c = 15.8438(13) Å, U = 2744.6(4) Å^3, Z = 4, D_c = 1.919 Mg m^{-3}, μ(Cu-Kα) = 3.086 mm^{-1}, T = 123 K. Total 19 705 reflections, 4905 unique, R_{int} = 0.051. Refinement of 4869 reflections (434 parameters) with $I > 2\sigma(I)$ converged at final R_1 = 0.0369 (R_1 all data = 0.0370), wR_2 = 0.1038 (wR_2 all data = 0.1038), gof = 1.0014. CCDC 1062412.†

DSC preparation. The fabrication method for the DSCs was based on that of Grätzel.[38,39] Solaronix Test Cell Titania Electrodes were used for the photoanodes. They were washed with EtOH and sintered at 450 °C for 30 min, then cooled to ≈80 °C and immersed in a 1.0 mM DMSO solution of **4** (Scheme 4) for 24 h at room temperature. The colourless electrodes were removed from the solution, washed with DMSO and EtOH and dried in a nitrogen stream. Each electrode was then immersed for 3 days in a CH_2Cl_2 solution of [Cu(**2**)$_2$][PF$_6$] or [Cu(**3**)$_2$][PF$_6$] (0.1 mM); during this period, the electrodes turned red-orange and the colour persisted when the electrodes were removed, washed with CH_2Cl_2 and dried with a nitrogen stream. An N719 reference electrode was made by immersing a Solaronix Test Cell Titania Electrode in a 0.3 mM EtOH solution of N719 (Solaronix) for 3 days. The electrode was then removed, washed with EtOH and dried with a nitrogen stream. For the counter electrodes, Solaronix Test Cell Platinum Electrodes were used, and volatile organic impurities were removed by heating on a heating plate (450 °C, 30 min).

The dye-covered TiO_2 electrode and Pt counter-electrode were combined using thermoplast hot-melt sealing foil (Solaronix Test Cell Gaskets) by heating while pressing them together. The electrolyte (LiI (0.1 M), I_2 (0.05 M), 1-methylbenzimidazole (0.5 M), 1-butyl-3-methylimidazolinium iodide (0.6 M) in 3-

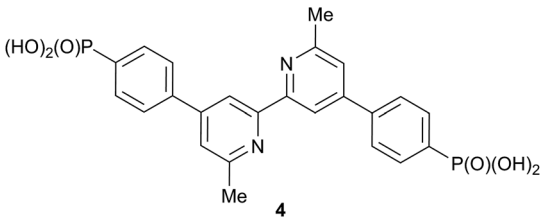

4

Scheme 4 Structure of the anchoring ligand **4** used in DSCs.

methoxypropionitrile) was introduced into the DSC by vacuum backfilling. The hole in the counter electrode was sealed with hot-melt sealing foil (Solaronix Test Cell Sealings) and a cover glass (Solaronix Test Cell Caps).

Measurements were made by irradiating from behind using a light source LOT Quantum Design LS0811 (100 mW cm^{-2} = 1 sun). The power of the simulated light was calibrated using a reference Si cell. All DSCs were completely masked[40,41] before measurements were made.

For solid-state absorption spectra of adsorbed dyes, Solaronix Test Cell Titania Electrodes (transparent) were used and the dye assembly was as described above for the photoanode.

External quantum efficiencies. External quantum efficiency (EQE) measurements were made using a Spe-Quest quantum efficiency instrument from Rera Systems (Netherlands) with a 100 W halogen lamp (QTH) and a lambda 300 grating monochromator (Lot Oriel). The monochromatic light was modulated to 3 Hz using a chopper wheel (ThorLabs). The cell response was amplified with a large dynamic range IV converter (CVI Melles Griot) and measured with a SR830 DSP Lock-In amplifier (Stanford Research).

DFT calculations. Ground state density functional theory (DFT) calculations were performed using Spartan 14 (v. 1.1.8)[42] at the B3LYP level with a 6-31G* basis set in vacuum. Initial structure minimization was carried out at a molecular mechanics level.

Results and discussion

Preparation and characterization of 3

The asymmetrical ligand **3** was prepared under microwave conditions by the Negishi cross coupling[43] of 2-chloro-6-(trifluoromethyl)pyridine and 2-pyridylzinc bromide in the presence of a catalytic amount of $[Pd(PPh_3)_4]$. After workup, **3** was isolated in 61% yield. The base peak in the electrospray mass spectrum appeared at *m*/*z* 225.1 and arose from $[M + H]^+$. The ^1H and ^{13}C NMR spectra (assigned by 2D methods) of a CD_2Cl_2 solution of **3** were consistent with the structure shown in Scheme 3. In the ^1H NMR spectrum of **3** (Fig. 1), the resonances from the CF_3-substituted pyridine ring (δ 8.64, 7.99 and 7.69 ppm) are close to those observed for disubstituted **2** (ref. 34) (Scheme 3) in the same solvent (δ 8.73, 8.03 and 7.74 ppm). A singlet at δ −68.4 ppm was observed in the ^{19}F NMR spectrum of **3** (the same chemical shift exhibited by ligand **2**) and coupling to C^{CF3} (J_{CF} = 274 Hz) and C^{A6} (J_{CF} = 35 Hz) in the ^{13}C NMR spectrum of **3** was consistent with the reported values of J_{CF} in **2**.[34] Coupling from the CF_3 group to C^{A5} (J_{CF} = 2.9 Hz) was also resolved.

Synthesis and characterization of $[Cu(2)_2][PF_6]$ and $[Cu(3)_2][PF_6]$

The homoleptic complexes $[Cu(2)_2][PF_6]$ and $[Cu(3)_2][PF_6]$ were prepared by the reaction of $[Cu(MeCN)_4][PF_6]$ with two equivalents of the respective ligand in CH_2Cl_2. Use of MeCN, both in the synthesis and spectroscopic characterization, was avoided because of possible competitive coordination to copper.[44] The base peak in the MALDI-TOF mass spectrum of each complex was assigned to the $[CuL_2]^+$ ion (*m*/*z* 647.2 for L **2**, *m*/*z* 511.1 for L = **3**). Fig. 2 shows the solution ^1H NMR spectra of the complexes; the ^1H and ^{13}C NMR spectra were assigned using 2D-methods and are consistent with the presence of a 6,6′-disubstituted ligand in $[Cu(2)_2][PF_6]$ and a 6-substituted ligand in $[Cu(3)_2][PF_6]$. The ^{19}F NMR spectra of $[Cu(2)_2][PF_6]$ and $[Cu(3)_2][PF_6]$ are shown in Fig. S1;† the relative integrals of the singlets for ligands **2** or **3** with respect to the doublet for the $[PF_6]^-$ ion are consistent with four or two CF_3 groups, respectively.

The solution absorption spectra of $[Cu(2)_2][PF_6]$ and $[Cu(3)_2][PF_6]$ are shown in Fig. 3 and data given in Table 1. The intense, high-energy transitions arise from ligand-based $\pi^* \leftarrow \pi$ transitions, and the broad band in the visible region from metal-to-ligand charge transfer (MLCT).[45,46] In $[Cu(2)_2][PF_6]$, the MLCT band has a maximum at 445 nm compared with 443 nm in $[Cu(3)_2][PF_6]$. This compares with 453 nm in $[Cu(1)_2][PF_6]$ (see Scheme 3 for **1**).[28] Similarly, the MLCT bands in $[Cu(dmp)_2][PF_6]$ and $[Cu(bfp)_2][PF_6]$ arise at similar wavelengths (453 and 462 nm, respectively).[28,30,47]

The electrochemical behaviour of $[Cu(2)_2][PF_6]$ was investigated in CH_2Cl_2 solution. Studies of the electrochemistry of $[Cu(phen)_2][PF_6]$ complexes demonstrated that donor solvents such as MeCN and DMF lower the Cu^+/Cu^{2+} potential because of solvent participation to give 5-coordinate copper(II) complexes.[48] For $[Cu(dmp)_2][PF_6]$, $E^{ox}_{1/2}$ shifts from 0.43 V in CH_2Cl_2 to 0.15 V in DMF (*versus* Fc/Fc^+ with $[^nBu_4N][PF_6]$ as supporting electrolyte).[48] An independent measurement gives $E^{ox}_{1/2}$ = 0.50 V for $[Cu(dmp)_2][PF_6]$ in CH_2Cl_2 and 0.27 V in MeCN (*versus* Fc/Fc^+ with $[^nBu_4N][PF_6]$ as supporting electrolyte).[49] We have previously reported $E^{ox}_{1/2}$ for $[Cu(1)_2][PF_6]$ as 0.17 V in MeCN (*versus* Fc/Fc^+);[28] in CH_2Cl_2, a reversible process at $E^{ox}_{1/2}$ = +0.44 V is observed. This shift to

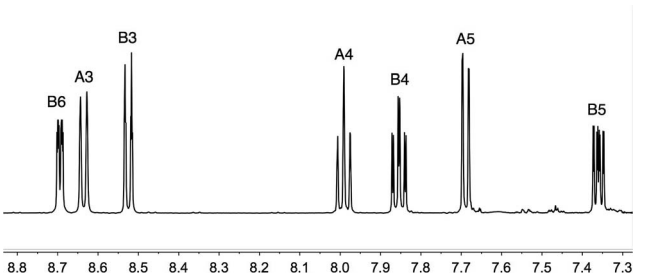

Fig. 1 500 MHz ^1H NMR spectrum of compound **3** in $CDCl_3$. Chemical shifts in δ/ppm. See Scheme 3 for ring labelling.

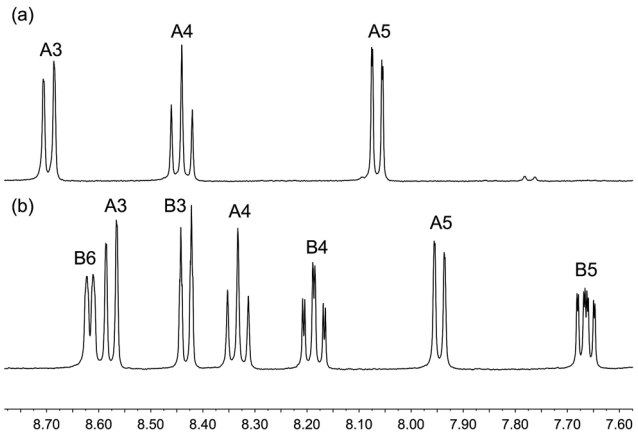

Fig. 2 500 MHz ^{1}H NMR spectra of (a) [Cu(**2**)$_2$][PF$_6$] and (b) [Cu(**3**)$_2$][PF$_6$] in CD_2Cl_2. Chemical shifts in δ/ppm. See Scheme 3 for ring labelling.

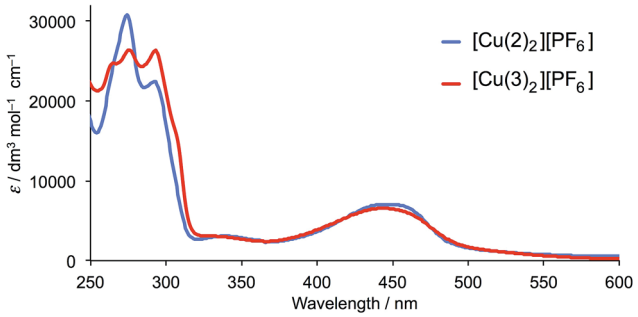

Fig. 3 Solution absorption spectra of [Cu(**2**)$_2$][PF$_6$] and [Cu(**3**)$_2$][PF$_6$] (CH_2Cl_2, 2.5 × 10^{-5} mol dm^{-3}).

higher potential is consistent with the solvent dependence of [Cu(dmp)$_2$][PF$_6$].[48,49] The cyclic voltammogram (CV) of [Cu(**1**)$_2$][PF$_6$] was referenced internally by adding ferrocene at the end of the experiment. A reversible oxidation process was observed in the CV of [Cu(**2**)$_2$][PF$_6$] in CH_2Cl_2. However, when ferrocene was added as an internal reference, a reversible Fc/Fc$^+$ wave was observed at an uncharacteristically low potential; the reason for this may lie in electron transfer between Cu^{2+} and Cp_2Fe.[50,51] A value of $E^{ox}_{1/2}$ = +0.72 V for [Cu(**2**)$_2$][PF$_6$] (Fig. 4) was determined using an external Fc/Fc$^+$ reference. The replacement of four Me by CF_3 groups results in the expected higher potential for Cu^+ oxidation, and is consistent with the trend on going from [Cu(dmp)$_2$][PF$_6$] to [Cu(bfp)$_2$][PF$_6$] (see Scheme 1); for the latter, a value of $E^{ox}_{1/2}$ = +1.55 V is reported *versus* SCE,[30] ≈1.17 V *versus* Fc/Fc$^+$ using the conversion of Pavlishchuk and Addison.[52] No well resolved reduction processes were observed for [Cu(**2**)$_2$][PF$_6$] within the solvent-accessible window (Fig. 4).

Crystal structure of [Cu(2)$_2$][PF$_6$]

Single crystals of [Cu(**2**)$_2$][PF$_6$] were grown from CH_2Cl_2 by diffusion of Et_2O, and the structure of the [Cu(**2**)$_2$]$^+$ cation is shown in Fig. 5. The copper(I) atom adopts the expected tetrahedral coordination environment with two chelating ligands **2**, and bond parameters for the coordination sphere are listed in the caption to Fig. 5. One bpy domain is planar (angle between the least squares planes through the rings containing N1 and N2 = 1.0°) while the second ligand is twisted (angle between the planes through the rings with N3 and N24 = 9.0°) leading to a small helical twist (Fig. 6a) that renders the cation chiral. The chirality is defined in terms of the orientation of the CF_3 groups containing atoms C12 and C24; one lies above and one below the least squares plane of the bpy unit to which they are bonded. The complex crystallizes in the non-centrosymmetric space group $P2_12_12_1$ and we propose that the steric demands of the CF_3 groups (Fig. 6b) prevent racemization in the solid state. Significantly, [Cu(bfp)$_2$][BF$_4$] and [Cu(bfp)$_2$][PF$_6$][30] (see Scheme 1) also crystallize in the space group $P2_12_12_1$. As discussed by Kovalevsky *et al.* for [Cu(bfp)$_2$]$^+$ in which the phen domains are close to orthogonal,[31] the steric requirements of the CF_3 groups prevent significant flattening of the tetrahedral coordination sphere in [Cu(**2**)$_2$]$^+$. The angle between the least squares planes through the two bpy domains in [Cu(**2**)$_2$]$^+$ is 84.1°, compared to 74.3° in [Cu(**1**)$_2$][PF$_6$].[28]

Ligand exchange between [Cu(1)$_2$]$^+$ and [Cu(2)$_2$]$^+$

On-surface assembly of the copper(I) dyes [Cu(**4**)(**2**)]$^+$ and [Cu(**4**)(**3**)]$^+$ (see below) depends upon ligand exchange between surface-bound **4** with 6,6′-dimethyl substituents (Scheme 4) and

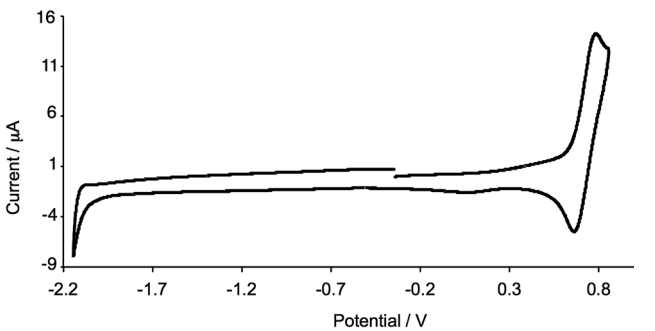

Fig. 4 Cyclic voltammogram of [Cu(**3**)$_2$][PF$_6$] in CH_2Cl_2 (referenced externally to Fc/Fc$^+$). Scan rate = 300 mV s^{-1}; Pt working electrode.

Table 1 Solution absorption maxima for [Cu(**2**)$_2$][PF$_6$] and [Cu(**3**)$_2$][PF$_6$] in CH_2Cl_2

Complex	λ_{max} (ε) $\pi^* \leftarrow \pi$/nm (dm^3 mol^{-1} cm^{-1})	λ_{max} (ε) MLCT/nm (dm^3 mol^{-1} cm^{-1})
[Cu(**2**)$_2$][PF$_6$]	273 (30 500), 295 (23 000), 340 (2980)	445 (7050)
[Cu(**3**)$_2$][PF$_6$]	263 (24 400), 273 (25 800), 293 (26 200), 340 (2940)	443 (6580)

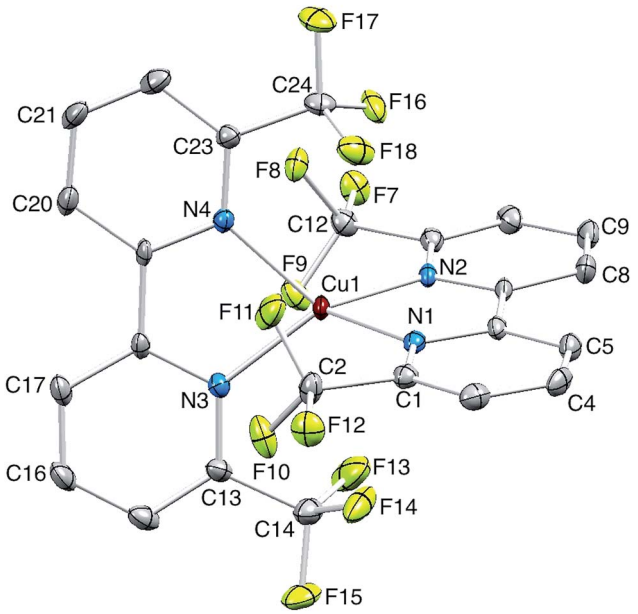

Fig. 5 Structure of the $[Cu(\mathbf{2})_2]^+$ cation in $[Cu(\mathbf{2})_2][PF_6]$; H atoms omitted and ellipsoids plotted at 30% probability level. Selected bond parameters: Cu1–N1 = 2.036(3), Cu1–N2 = 2.021(3), Cu1–N3 = 2.030(3), Cu1–N4 = 2.027(3) Å; N1–Cu1–N2 = 82.41(11), N1–Cu1–N3 = 124.71(12), N2–Cu1–N3 = 127.02(11), N1–Cu1–N4 = 123.51(11), N2–Cu1–N4 = 122.05(11), N3–Cu1–N4 = 82.85(12)°; C–F bond distances are in the range 1.319(5) to 1.341(4) Å.

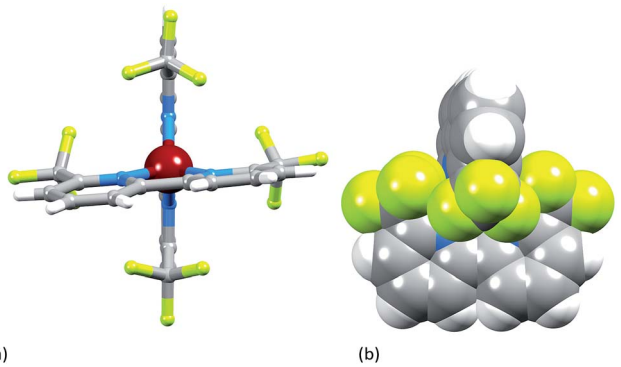

Fig. 6 (a) View of the $[Cu(\mathbf{2})_2]^+$ cation showing helical twist in one ligand; (b) space-filling diagram illustrating the shielding of the Cu1 atom by the four CF_3 groups.

the homoleptic complexes $[Cu(\mathbf{2})_2]^+$ and $[Cu(\mathbf{3})_2]^+$. To verify that the steric demands of the CF_3 groups did not impede this exchange, ^1H and ^{19}F NMR spectroscopies were used to monitor a CH_2Cl_2 solution containing $[Cu(\mathbf{1})_2][PF_6]$ and $[Cu(\mathbf{2})_2][PF_6]$; ligands **1** and **2** contain a 6,6′-dimethyl and 6,6′-bis(trifluoromethyl) substitution pattern, respectively. In Fig. 7, the ^1H NMR spectra of $[Cu(\mathbf{1})_2][PF_6]$ and $[Cu(\mathbf{2})_2][PF_6]$ are compared with the spectrum of a solution containing equimolar amounts of both compounds 15 minutes after mixing. The data confirm that ligand exchange occurs rapidly. The relative integrals of the signals for H^{Me}(homoleptic) : H^{Me}(heteroleptic) are 1.00 : 1.06, *i.e.* essentially a statistical mixture of homo- and heteroleptic complexes. The ^{19}F NMR spectrum of the mixture showed two resonances at δ −68.2 and −68.6 ppm arising from $[Cu(\mathbf{2})_2]^+$ and $[Cu(\mathbf{1})(\mathbf{2})]^+$, respectively, in addition to a doublet at δ −73.3 ppm from the $[PF_6]^-$ ion (Fig. S2†).

Dye adsorption and DSC performances

Transparent electrodes with adsorbed dyes were prepared by dipping the electrodes first in a solution of anchoring ligand **4** (Scheme 4) followed by a solution of either $[Cu(\mathbf{2})_2][PF_6]$ or $[Cu(\mathbf{3})_2][PF_6]$. The soaking times and solvents were the same as those used for preparing the photoanodes for the DSCs (see Experimental section). After the electrodes had been dried, their solid-state absorption spectra (transmission mode) were recorded (Fig. 8a). The MLCT band for both adsorbed dyes $[Cu(\mathbf{4})(\mathbf{2})][PF_6]$ and $[Cu(\mathbf{4})(\mathbf{3})][PF_6]$ appears at ≈455 nm, but the relative intensities of the MLCT bands indicate that dye coverage for $[Cu(\mathbf{4})(\mathbf{3})][PF_6]$ is greater than for $[Cu(\mathbf{4})(\mathbf{2})][PF_6]$. This difference was reproducible for a second set of electrodes soaked in the dye baths under the same conditions as the first set, and can also be seen by eye (Fig. 8b). The 0.1 mM CH_2Cl_2 solutions of $[Cu(\mathbf{2})_2][PF_6]$ and $[Cu(\mathbf{3})_2][PF_6]$ used in the second dye bath appear by eye to have the same yellow-orange colour and the same intensity of colour.

The dye-functionalized photoanodes for the DSCs were prepared by sequentially soaking the electrodes in solutions of anchoring ligand **4** followed by either $[Cu(\mathbf{2})_2][PF_6]$ or $[Cu(\mathbf{3})_2][PF_6]$. The process was the same as for the assembly of surface-bound $[Cu(\mathbf{4})(\mathbf{1})]^+$ previously reported.[29] Duplicate cells were prepared for each dye and the cell characteristics are shown in Table 2; the data are compared to those of cells containing $[Cu(\mathbf{4})(\mathbf{1})]^+$ and to a reference cell containing N719. All cells were fully masked to prevent overestimation of their

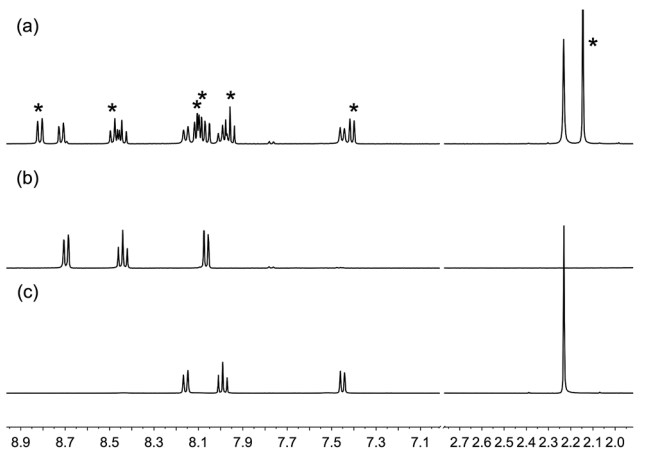

Fig. 7 500 MHz ^1H NMR spectra of CD_2Cl_2 solutions of (a) $[Cu(\mathbf{1})_2][PF_6]$ and $[Cu(\mathbf{2})_2][PF_6]$ 15 minutes after mixing; peaks due to $[Cu(\mathbf{1})(\mathbf{2})]^+$ are shown with *; (b) $[Cu(\mathbf{2})_2][PF_6]$; (c) $[Cu(\mathbf{1})_2][PF_6]$. The initial solution for (a) contained 0.38 mmol of each of $[Cu(\mathbf{1})_2][PF_6]$ and $[Cu(\mathbf{2})_2][PF_6]$. Chemical shifts in δ/ppm. Note that in the mixture shown in (a), signals for **1** in $[Cu(\mathbf{1})_2][PF_6]$ are slightly broader than those **1** in $[Cu(\mathbf{1})(\mathbf{2})][PF_6]$; for the Me signals, FWHM = 9 Hz in $[Cu(\mathbf{1})_2][PF_6]$ and 7 Hz in $[Cu(\mathbf{1})(\mathbf{2})][PF_6]$.

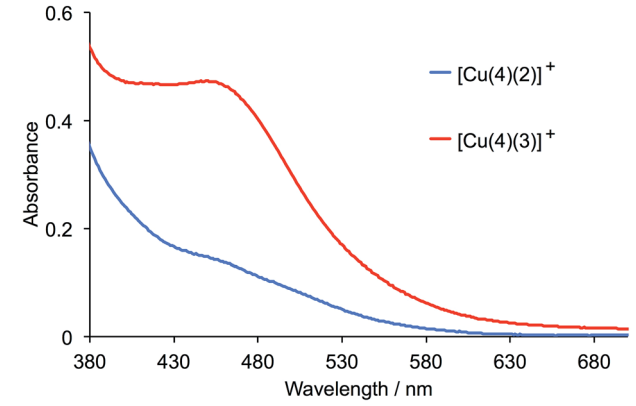

(a)

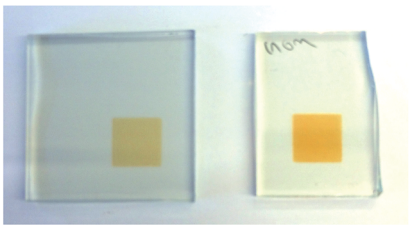

(b)

Fig. 8 (a) Solid-state absorption spectra of transparent TiO_2 electrodes functionalized with the dyes $[Cu(4)(2)]^+$ and $[Cu(4)(3)]^+$. (b) Photographs of the two electrodes with dyes $[Cu(4)(2)]^+$ (left) and $[Cu(4)(3)]^+$ (right).

performances.[40,41] Although efficiency values, η, are typically quoted in the literature, we now routinely also include values relative to N719 measured under the same conditions (last column of Table 2). This is a convenient and valid means to compare measurements made in different laboratories, with different coworkers and with different commercial sun simulators.[29] The reproducibility of the DSCs containing N719 between cells fabricated previously[29] and in this work (Table 2) serves to validate the results for the copper(I) dyes in both investigations.

Firstly, we consider the parameters in Table 2 for the DSCs on the day of fabrication. Good fill factors (ff, ≈70–75%) for all the copper(I) dye-containing cells are observed. The short-circuit current density (J_{SC}) and open-circuit voltage (V_{OC}) values are validated by the reproducibility between each pair of duplicate cells (Fig. 9). The introduction of the fluoro-substituents on going from $[Cu(4)(1)]^+$ to $[Cu(4)(2)]^+$ or $[Cu(4)(3)]^+$ results in a significant increase in J_{SC} and a small increase in V_{OC}. The enhanced J_{SC} with introduction of fluoro-substituents is the opposite trend to that observed by Diau and coworkers[26] upon fluorination of the aryl substituent in the ruthenium(II) dye shown in Scheme 5. Interestingly, the best performing of the copper(I) dyes are those with ligand **3** (one CF_3) group, and this is consistent with the higher dye-loading for $[Cu(4)(3)]^+$ with respect to $[Cu(4)(2)]^+$ evidenced from the solid-state absorption spectra (Fig. 8a). All cells exhibit a photoconversion efficiency (η) of ≈30–34% relative to N719 set at 100%, which is a notable improvement with respect to DSCs containing $[Cu(4)(1)]^+$ with no fluoro-groups (right column, Table 2).

Table 2 Parameters of masked DSCs with $[Cu(4)(2)]^+$ and $[Cu(4)(3)]^+$ compared to a reference DSC containing N719, and previously reported data for $[Cu(4)(1)]^+$ measured under the same conditions using a LOT Quantum Design LS0811 as the light source

Dye	J_{SC}/mA cm^{-2}	V_{OC}/mV	ff/%	η/%	Relative[a] η/%
On the day of sealing the cells					
$[Cu(4)(2)]^+$	4.81	537	73.5	1.90	31.8
$[Cu(4)(2)]^+$	4.67	531	71.5	1.78	30.0
$[Cu(4)(3)]^+$	5.35	530	73.4	2.08	34.8
$[Cu(4)(3)]^+$	5.40	532	70.3	2.02	33.8
N719[c]	13.65	652	67.0	5.97	100
$[Cu(4)(1)]^+$	3.79	522	73.8	1.46	24.7[b]
$[Cu(4)(1)]^+$	3.46	527	74.3	1.35	22.8[b]
N719[d]	12.51	672	70.2	5.91	100
1 day after sealing the cells					
$[Cu(4)(2)]^+$	4.73	557	73.8	1.95	33.2
$[Cu(4)(2)]^+$	4.63	550	70.6	1.80	30.6
$[Cu(4)(3)]^+$	5.45	540	73.0	2.15	36.6
$[Cu(4)(3)]^+$	5.56	546	70.2	2.13	36.2
N719[c]	13.19	681	65.5	5.88	100
3 days after sealing the cells					
$[Cu(4)(2)]^+$	4.85	564	73.4	2.00	33.6
$[Cu(4)(2)]^+$	4.68	559	70.7	1.85	31.1
$[Cu(4)(3)]^+$	5.17	541	73.2	2.05	34.5
$[Cu(4)(3)]^+$	5.53	562	70.2	2.18	36.6
N719[c]	13.16	689	65.6	5.95	100
8 days after sealing the cells					
$[Cu(4)(2)]^+$	4.77	565	73.2	1.97	32.5
$[Cu(4)(2)]^+$	4.70	556	67.7	1.77	29.2
$[Cu(4)(3)]^+$	5.48	563	70.8	2.18	35.9
$[Cu(4)(3)]^+$	5.81	567	68.6	2.26	37.2
N719[c]	12.82	696	68.1	6.07	100

[a] Relative to N719 efficiency set at 100%. [b] Data from ref. 29. [c] N719 reference for the current study. [d] N719 reference for the previous study.[29]

The cell parameters were measured several times over a period of 8 days after DSC fabrication (Table 2) and *J–V* curves for the best performing DSCs (Fig. 10) show a marked and similar improvement in V_{OC} for the two dyes (537 to 565 mV for $[Cu(4)(2)]^+$, and 532 to 567 mV for $[Cu(4)(3)]^+$). The dye with one CF_3 group also gains in J_{SC}, and the resulting global efficiency is 37.2% relative to N719 set at 100%.

The external quantum efficiency (EQE) spectra for DSCs containing $[Cu(4)(2)]^+$ and $[Cu(4)(3)]^+$ are shown in Fig. 11, and a comparison of these spectra with the solid state UV-Vis spectra shown in Fig. 8 demonstrates the proportion of the absorbed light that is converted to electrical current. Both dyes exhibit a maximum EQE at 480 nm, with EQE_{max} values of 46% for $[Cu(4)(2)]^+$ and 51% for $[Cu(4)(3)]^+$. This compares with 69% at 480 nm for N719. An EQE_{max} of 51% is very pleasing for a copper(I) sensitizer, and is comparable to those reported for the record dye of Boujtita and Odobel,[17] and for the iodo-substituted dye previously reported.[21] However, it is clear from

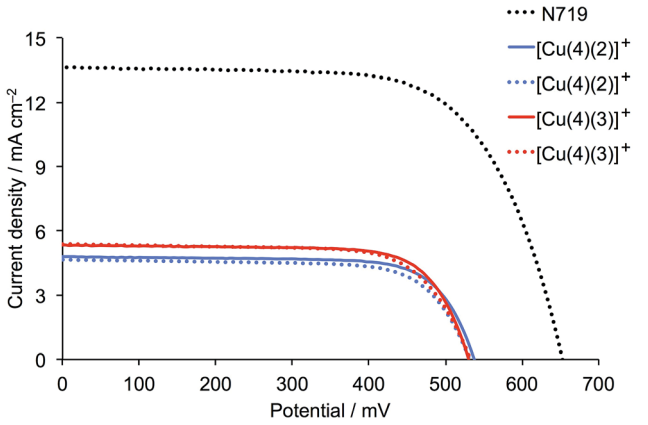

Fig. 9 *J–V* curves for duplicate DSCs containing dyes $[Cu(\mathbf{4})(\mathbf{2})]^+$ and $[Cu(\mathbf{4})(\mathbf{3})]^+$ compared to reference dye N719. The parameters are for the day of sealing the DSCs (top of Table 2).

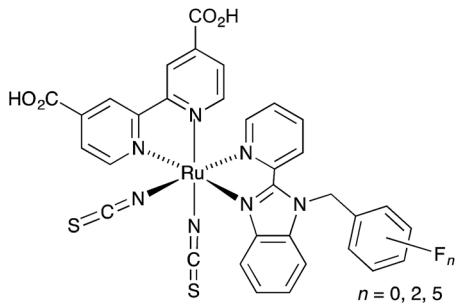

Scheme 5 Ruthenium(II) dyes used by Diau to investigate the effects of fluoro-substitution on DSC performance.[26]

Fig. 11 that light-harvesting in the red-part of the spectrum remains deficient in $[Cu(\mathbf{4})(\mathbf{2})]^+$ and $[Cu(\mathbf{4})(\mathbf{3})]^+$.

DFT calculations

Ground state density functional theory (DFT) calculations were carried out on $[Cu(\mathbf{4})(\mathbf{1})]^+$,[29] $[Cu(\mathbf{4})(\mathbf{2})]^+$ and $[Cu(\mathbf{4})(\mathbf{3})]^+$ to

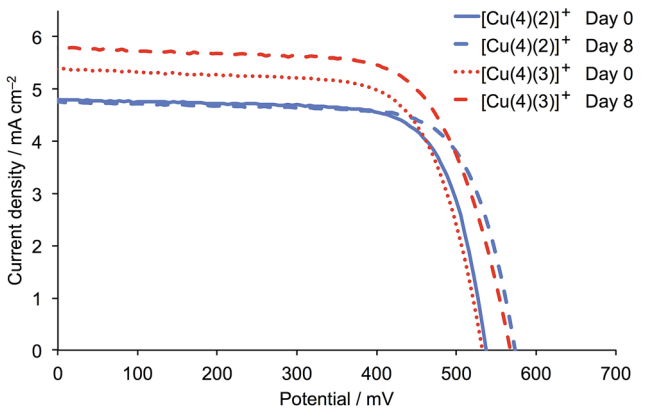

Fig. 10 *J–V* curves for the best performing DSCs (from Table 2) containing the dyes $[Cu(\mathbf{4})(\mathbf{2})]^+$ and $[Cu(\mathbf{4})(\mathbf{3})]^+$ on the day of sealing the DSCs (day 0) and a week later. Colour and line coding on day 0 is consistent with Fig. 9.

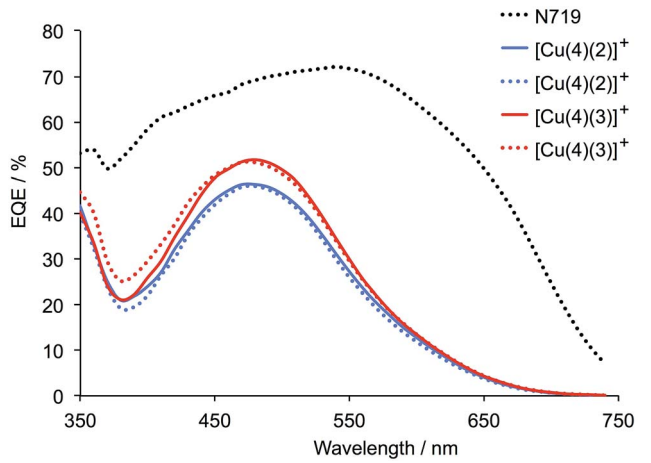

Fig. 11 EQE spectra for duplicate DSCs containing dyes $[Cu(\mathbf{4})(\mathbf{2})]^+$ and $[Cu(\mathbf{4})(\mathbf{3})]^+$ compared to reference dye N719. The spectra were recorded on the day of sealing the DSCs.

compare the orbital compositions of MOs in the HOMO–LUMO manifold. The choice of basis set was made following a more detailed investigation of the effects of different basis sets in related copper(I) complexes.[28] We focus only on trends of the MO characters on introducing the fluoro-substituents.

On going from $[Cu(\mathbf{4})(\mathbf{1})]^+$ to $[Cu(\mathbf{4})(\mathbf{2})]^+$ to $[Cu(\mathbf{4})(\mathbf{3})]^+$, both the HOMO and LUMO are stabilized. This is consistent with the calculated trend on going from $[Cu(dmp)_2]^+$ to $[Cu(bfp)_2]^+$,[33] and stabilization of the HOMO from $[Cu(\mathbf{4})(\mathbf{1})]^+$ to $[Cu(\mathbf{4})(\mathbf{2})]^+$ is consistent with the shift to more positive oxidation potential observed from $[Cu(\mathbf{1})_2]^+$ to $[Cu(\mathbf{2})]^+$ (see above).

The compositions of the highest lying MOs and lowest lying virtual MOs in each of the heteroleptic complexes are depicted in Fig. 12. The HOMO and HOMO−1 are close in energy and, taken as a pair, their characters are similar in all three complexes. Both MOs are based on the copper with contributions from the ancillary ligand (HOMO in $[Cu(\mathbf{4})(\mathbf{1})]^+$ or HOMO−1 in $[Cu(\mathbf{4})(\mathbf{2})]^+$ and $[Cu(\mathbf{4})(\mathbf{3})]^+$) or from both bpy domains (HOMO−1 in $[Cu(\mathbf{4})(\mathbf{1})]^+$ or HOMO in $[Cu(\mathbf{4})(\mathbf{2})]^+$ and $[Cu(\mathbf{4})(\mathbf{3})]^+$). As previously reported,[29] the LUMO of $[Cu(\mathbf{4})(\mathbf{1})]^+$ is localized on anchoring ligand **4**, as desired for accepting an electron in the excited state prior to injection into the semiconductor. As Fig. 12 shows, the characters of the three lowest lying unoccupied MOs in $[Cu(\mathbf{4})(\mathbf{1})]^+$, $[Cu(\mathbf{4})(\mathbf{2})]^+$ and $[Cu(\mathbf{4})(\mathbf{3})]^+$ are bpy-based, either on the anchoring or ancillary ligand. Changes in the orbital compositions alone in the HOMO–LUMO manifold do not explain why dyes $[Cu(\mathbf{4})(\mathbf{2})]^+$ and $[Cu(\mathbf{4})(\mathbf{3})]^+$ perform better than $[Cu(\mathbf{4})(\mathbf{1})]^+$. It is likely that the stabilization of the HOMO and LUMO which accompanies the introduction of the CF_3 groups is key to the enhanced dye performance, and/or that electron recombination processes are hindered. We are currently undertaking an electrochemical impedance spectroscopic investigation of a range of copper(I) sensitizers in order to gain insight into relationships between 6,6′-substituted 2,2′-bipyridine ancillary ligands and trends in DSC performances.

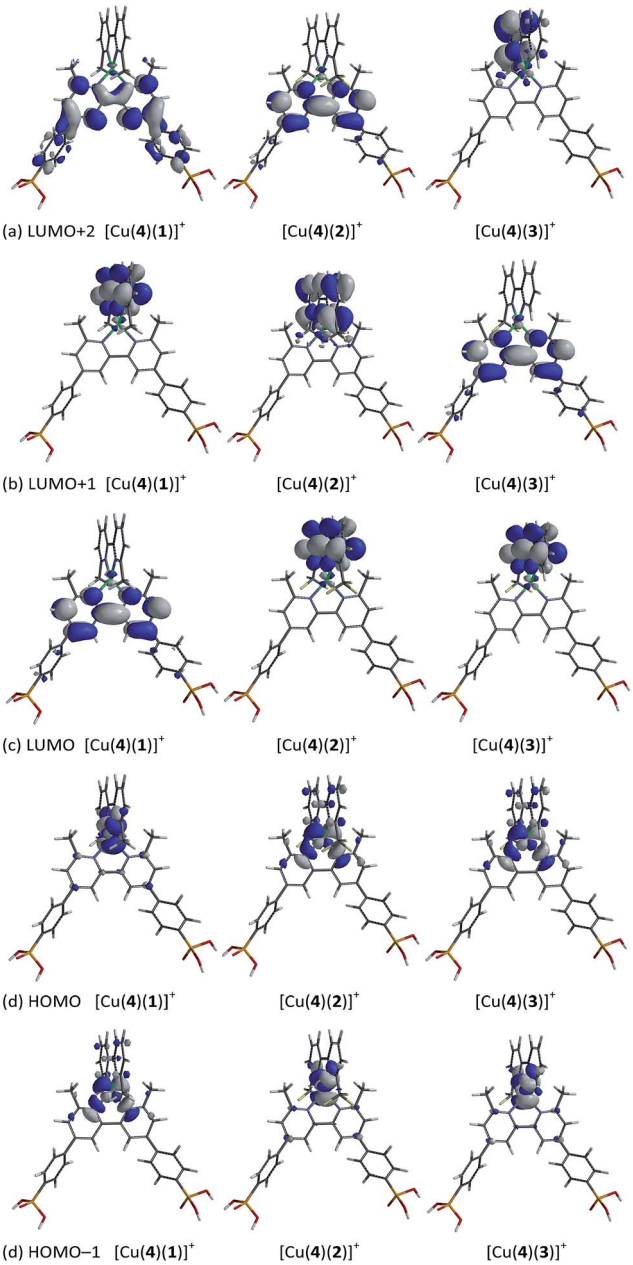

Fig. 12 Calculated compositions of MOs in the HOMO–LUMO manifolds of $[[Cu(\mathbf{4})(\mathbf{1})]^+$, $[Cu(\mathbf{4})(\mathbf{2})]^+$ and $[Cu(\mathbf{4})(\mathbf{3})]^+$. (a) LUMO+2, (b) LUMO+1, (c) LUMO, (d) HOMO and (e) HOMO−1. In each diagram, the anchoring ligand **4** is at the bottom.

Conclusions

The complexes $[Cu(\mathbf{2})_2][PF_6]$ and $[Cu(\mathbf{3})_2][PF_6]$ bearing trifluoromethyl substituents have been investigated, and the single crystal structure of $[Cu(\mathbf{2})_2][PF_6]$ has been determined. The Cu^+/Cu^{2+} redox couple shifts to higher potential (+0.44 to +0.72 V *versus* Fc/Fc^+ in CH_2Cl_2) on replacing methyl groups in $[Cu(\mathbf{1})_2][PF_6]$ by CF_3 groups in $[Cu(\mathbf{2})_2][PF_6]$. ^1H and ^{19}F NMR spectra for a CH_2Cl_2 solution of $[Cu(\mathbf{1})_2][PF_6]$ and $[Cu(\mathbf{2})_2][PF_6]$ show that the ligands in $[Cu(\mathbf{2})_2][PF_6]$ remain very labile. The copper(I) dyes $[Cu(\mathbf{4})(\mathbf{2})]^+$ and $[Cu(\mathbf{4})(\mathbf{3})]^+$ have been assembled on TiO_2 electrodes using a stepwise on-surface method, and DSCs containing the fluorinated ancillary ligands exhibit excellent photoconversion efficiencies of ≈30–34% relative to N719 set at 100%; this is a noteworthy improvement with respect to DSCs containing $[Cu(\mathbf{4})(\mathbf{1})]^+$, showing that fluoro-substitution is beneficial. Stabilization of the HOMO in the fluorinated-dyes is confirmed by DFT calculations; the compositions of the MOs in the HOMO–LUMO manifold are little changed. The improved DSC performances arise from improved J_{SC} values for $[Cu(\mathbf{4})(\mathbf{3})]^+$ and $[Cu(\mathbf{4})(\mathbf{2})]^+$ *versus* $[Cu(\mathbf{4})(\mathbf{1})]^+$, consistent with high EQE_{max} values of 46% for $[Cu(\mathbf{4})(\mathbf{2})]^+$ and 51% for $[Cu(\mathbf{4})(\mathbf{3})]^+$ (both at $\lambda_{max} = 480$ nm).

Abbreviations

dmp	2,9-Dimethyl-1,10-phenanthroline
bfp	2,9-Bis(trifluoromethyl)-1,10-phenanthroline

Acknowledgements

We thank the Swiss National Science Foundation (Grant number 200020_144500), the European Research Council (Advanced Grant 267816 LiLo) and the University of Basel for financial support. Professor Howard Flack is acknowledged for helpful discussion. PD Dr Daniel Häussinger is acknowledged for assistance with ^{19}F NMR spectroscopy.

Notes and references

1 B. Bozic-Weber, E. C. Constable and C. E. Housecroft, *Coord. Chem. Rev.*, 2013, **257**, 3089.
2 M. S. Lazorski and F. N. Castellano, *Polyhedron*, 2014, **82**, 57.
3 F. Dumur, *Org. Electron.*, 2015, **21**, 27.
4 D. Volz, M. Wallesch, C. Fléchon, M. Danz, A. Verma, J. M. Navarro, D. M. Zink, S. Bräse and T. Baumann, *Green Chem.*, 2015, **17**, 1988.
5 R. D. Costa, E. Ortí, H. J. Bolink, F. Monti, G. Accorsi and N. Armaroli, *Angew. Chem., Int. Ed.*, 2012, **51**, 8178.
6 A. Yella, H.-W. Lee, H. N. Tsao, C. Yi, A. K. Chandiran, M. K. Nazeeruddin, E. W.-G. Diau, C.-Y. Yeh, S. M. Zakeeruddin and M. Grätzel, *Science*, 2011, **334**, 629; M. Zhang, Y. Wang, M. Xu, W. Ma, R. Li and P. Wang, *Energy Environ. Sci.*, 2013, **6**, 2944; K. Kakiage, Y. Aoyama, T. Yano, T. Otsuka, T. Kyomen, M. Unno and M. Hanaya, *Chem. Commun.*, 2014, **50**, 6379; H. Ozawa, Y. Okuyama and H. Arakawa, *ChemPhysChem*, 2014, **15**, 1201.
7 G. C. Vougioukalakis, A. I. Philippopoulos, T. Stergiopoulos and P. Falaras, *Coord. Chem. Rev.*, 2011, **255**, 2602.
8 A. Alonso-Vante, J. F. Nierengarten and J. P. Sauvage, *J. Chem. Soc., Dalton Trans.*, 1994, 1650.
9 S. Sakaki, T. Kuroki and T. Hamada, *Dalton Trans.*, 2002, 840.
10 T. Bessho, E. C. Constable, M. Graetzel, A. Hernandez Redondo, C. E. Housecroft, W. Kylberg, M. K. Nazeeruddin, M. Neuburger and S. Schaffner, *Chem. Commun.*, 2008, 3717.

11 E. C. Constable, A. Hernandez Redondo, C. E. Housecroft, M. Neuburger and S. Schaffner, *Dalton Trans.*, 2009, 6634.
12 See for example: Y.-J. Yuan, Z.-T. Yu, J.-Y. Zhang and Z.-G. Zou, *Dalton Trans.*, 2012, 9594; A. Colombo, C. Dragonetti, D. Roberto, A. Valore, P. Biagini and F. Melchiorre, *Inorg. Chim. Acta*, 2013, **407**, 204; K. A. Wills, H. J. Mandujano-Ramírez, G. Merino, D. Mattia, T. Hewat, N. Robertson, G. Oskam, M. D. Jones, S. E. Lewis and P. J. Cameron, *RSC Adv.*, 2013, **3**, 23361.
13 D. R. McMillin and K. M. McNett, *Chem. Rev.*, 1998, **98**, 1201.
14 A. Hernandez Redondo, E. C. Constable and C. E. Housecroft, *Chimia*, 2009, **63**, 205.
15 M. Schmittel and A. Ganz, *Chem. Commun.*, 1997, 999; M. Schmittel, H. Ammon, V. Kalsani, A. Wiegrefe and C. Michel, *Chem. Commun.*, 2002, 2566.
16 M. Sandroni, M. Kayanuma, A. Planchat, N. Szuwarski, E. Blart, Y. Pellegrin, C. Daniel, M. Boujtita and F. Odobel, *Dalton Trans.*, 2013, 10818.
17 M. Sandroni, L. Favereau, A. Planchat, H. Akdas-Kilig, N. Szuwarski, Y. Pellegrin, E. Blart, H. le Bozec, M. Boujtita and F. Odobel, *J. Mater. Chem. A*, 2014, **2**, 9944.
18 B. Bozic-Weber, E. C. Constable, C. E. Housecroft, P. Kopecky, M. Neuburger and J. A. Zampese, *Dalton Trans.*, 2011, 12584.
19 E. Schönhofer, B. Bozic-Weber, C. J. Martin, E. C. Constable, C. E. Housecroft and J. A. Zampese, *Dyes Pigm.*, 2015, **115**, 154.
20 S. Y. Brauchli, F. J. Malzner, E. C. Constable and C. E. Housecroft, *RSC Adv.*, 2014, **4**, 62728.
21 F. J. Malzner, S. Y. Brauchli, E. C. Constable, C. E. Housecroft and M. Neuburger, *RSC Adv.*, 2014, **4**, 48712.
22 See for example: S.-L. Wu, H.-P. Lu, H.-T. Yu, S.-H. Chuang, C.-L. Chiu, C.-W. Lee, E. W.-G. Diau and C.-Y. Yeh, *Energy Environ. Sci.*, 2010, **3**, 949 and references therein.
23 B. Bozic-Weber, S. Y. Brauchli, E. C. Constable, S. O. Fürer, C. E. Housecroft and I. A. Wright, *Phys. Chem. Chem. Phys.*, 2013, **15**, 4500.
24 S. Y. Brauchli, B. Bozic-Weber, E. C. Constable, N. Hostettler, C. E. Housecroft and J. Zampese, *RSC Adv.*, 2014, **4**, 34801.
25 S. Y. Brauchli, E. C. Constable and C. E. Housecroft, *Dyes Pigm.*, 2015, **113**, 447.
26 W.-K. Huang, H.-P. Wu, P.-L. Lin, Y.-P. Lee and E. W.-G. Diau, *J. Phys. Chem. Lett.*, 2012, **3**, 1830.
27 G. Marzani, J. Durantini, D. Minudri, M. Gervaldo, L. Otero, F. Fungo, G. Pozzi, M. Cavazzini, S. Orlandi and S. Quici, *J. Phys. Chem. C*, 2012, **116**, 21190.
28 B. Bozic-Weber, V. Chaurin, E. C. Constable, C. E. Housecroft, M. Meuwly, M. Neuburger, J. A. Rudd, E. Schönhofer and L. Siegfried, *Dalton Trans.*, 2012, 14157.
29 F. J. Malzner, S. Y. Brauchli, E. Schönhofer, E. C. Constable and C. E. Housecroft, *Polyhedron*, 2014, **82**, 116.
30 M. T. Miller, P. K. Gantzel and T. B. Karpishin, *Angew. Chem., Int. Ed.*, 1998, **37**, 1556.
31 A. Y. Kovalevsky, M. Gembicky and P. Coppens, *Inorg. Chem.*, 2004, **43**, 8282.
32 X. Wang, W. Wang, M. Koyama, M. Kubo and A. Miyamoto, *J. Photochem. Photobiol., A*, 2006, **179**, 149.
33 L.-Y. Zou, M.-S. Ma, Z.-L. Zhang, H. Li, Y.-X. Cheng and A.-M. Ren, *Org. Electron.*, 2012, **13**, 2627.
34 K. S. Chan and A. K.-S. Tse, *Synth. Commun.*, 1993, **23**, 1929.
35 G. J. Kubas, *Inorg. Synth.*, 1979, **19**, 90.
36 *APEX2, version 2 User Manual, M86-E01078*, Bruker Analytical X-ray Systems, Inc., Madison, WI, 2006.
37 P. W. Betteridge, J. P. Carruthers, R. I. Cooper, K. Prout and D. J. Watkin, *J. Appl. Crystallogr.*, 2003, **36**, 1487.
38 S. Ito, P. Chen, P. Comte, M. K. Nazeeruddin, P. Liska, P. Péchy and M. Grätzel, *Prog. Photovoltaics*, 2007, **15**, 603.
39 S. Ito, T. N. Murakami, P. Comte, P. Liska, C. Grätzel, M. K. Nazeeruddin and M. Grätzel, *Thin Solid Films*, 2008, **516**, 4613.
40 H. J. Snaith, *Energy Environ. Sci.*, 2012, **5**, 6513.
41 H. J. Snaith, *Nat. Photonics*, 2012, **6**, 337.
42 *Spartan'14*, Wavefunction, Inc., Irvine, CA 92612.
43 E. Negishi, *Angew. Chem., Int. Ed.*, 2011, **50**, 6738.
44 F. J. Malzner, S. Y. Brauchli, E. C. Constable, C. E. Housecroft and M. Neuburger, *RSC Adv.*, 2014, **4**, 48712.
45 M. W. Mara, K. A. Fransted and L. X. Chen, *Coord. Chem. Rev.*, 2015, **282–283**, 2 and references therein.
46 N. Armaroli, G. Accorsi, F. Cardinali and A. Listorti, *Top. Curr. Chem.*, 2007, **280**, 69 and references therein.
47 R. M. Everly and D. R. McMillin, *J. Phys. Chem.*, 1992, **95**, 9071.
48 M. Magni, A. Colombo, C. Dragonetti and P. Mussini, *Electrochim. Acta*, 2014, **141**, 324.
49 M. K. Eggleston, D. R. McMillin, K. S. Koenig and A. J. Pallenberg, *Inorg. Chem.*, 1997, **36**, 172.
50 J. Irangu, M. J. Ferguson and R. B. Jordan, *Inorg. Chem.*, 2005, **44**, 1619.
51 S. Itoh, N. Kishikawa, T. Suzuki and H. D. Takagi, *Dalton Trans.*, 2005, 1066.
52 V. V. Pavlishchuk and A. W. Addison, *Inorg. Chim. Acta*, 2000, **298**, 97.